Letter

Quantum bistability in the hyperfine ground state of atoms

B. Gábor [1,2] D. Nagy,[1] A. Vukics [1,*] and P. Domokos[1]
[1]*HUN-REN Wigner RCP, P.O. Box 49, H-1525 Budapest, Hungary*
[2]*Department of Theoretical Physics, University of Szeged, Tisza Lajos körút 84, H-6720 Szeged, Hungary*

(Received 30 March 2023; accepted 15 November 2023; published 11 December 2023)

First-order phase transitions are ubiquitous in nature; however, this notion is ambiguous and highly debated in the case of open quantum systems. We construct a paradigmatic example which allows for elucidating the key concepts. We show that atoms in an optical cavity can manifest a first-order dissipative phase transition where the stable coexisting phases are quantum states with high quantum purity. These states include atomic hyperfine ground states and coherent states of electromagnetic field modes. The scheme benefits from the collective enhancement of the coupling between the atoms and the cavity field. Thereby we propose a readily feasible experimental scheme to study the dissipative phase transition phenomenology in the quantum limit, allowing for, in particular, performing a finite-size scaling to the thermodynamic limit.

DOI: 10.1103/PhysRevResearch.5.L042038

First-order dissipative quantum phase transitions (DQPTs) [1,2] feature the following defining properties: (i) in a finite range of a given control parameter, the quantum system has multiple stable steady states, (ii) which are macroscopically discernible by an order parameter, and (iii) are approximately pure quantum states. When sweeping the control parameter across the critical domain, the steady state depends on the history, and the order parameter exhibits a hysteresis. It is condition (iii) which is exotic, and while many classical systems exhibit the multistability conditions (i) and (ii), it is only recently that examples for the quantum version have been found in various systems. A first-order DQPT was predicted theoretically for the clustering of Rydberg atoms [3–5], although the experimental feasibility has been contested [6–9]. Optical lattices with engineered losses [10,11], ultracold-atom cavity QED systems [12], nonlinear photonic or polaritonic modes [13,14], exciton-polariton condensates [15], and circuit QED systems [16–18] have also been shown to feature first-order dissipative phase transitions.

Optical bistability [19–23] is a paradigmatic example of a first-order phase transition in cavity QED. In its common form [20] it satisfies conditions (i) and (ii), but not (iii). The transmission of a laser-driven optical resonator mode can be suppressed or allowed at the same drive intensity, depending on the state of the atoms in the cavity mode. The nonlinearity originates from the saturation effect of two-level atoms. However, in the bright phase the saturated atoms correspond to a high-entropy mixed state, breaking condition (iii).

All three conditions are met in the case of the recently revealed photon-blockade breakdown (PBB) phase transition [24–26]. The experimental configuration is very similar, but the atomic medium comprises only a single two-level atom, and its electric dipole coupling with the mode has to be very large. This can be achieved in superconducting circuit QED systems in the microwave frequency regime where the signatures of a closely related bistability effect have been observed with three-level atoms [16].

In this paper we present an optical cavity QED scheme which manifests a first-order dissipative quantum phase transition in a transparent way and makes use of the collective enhancement of the coupling between the mode and an ensemble of atoms. Similarly to PBB, the thermodynamic limit where a bimodal phase-space distribution composed of two metastable states becomes true bistability between macroscopically distinct *phases* is reached by increasing the cooperativity. However, in contrast to PBB, this can be achieved by increasing not only the (single-atom) coupling constant—a feat that appears impossible in the optical domain—but also the atom number. This atom-number increase is not accompanied by an increase of the volume of the ensemble; spatial extension does not play an inherent role in the present scheme.

The proposed scheme is the extension of a recent experiment where we observed transmission blockade breakdown [27,28]; cf. also [29] for a related scenario: here we use two cavity modes instead of just one. The modes interact with an ensemble of atoms modeled by a four-level scheme. Besides the nonextensive character, the striking feature of the present scheme within the above listed zoo of first-order DPQTs is the high quantum purity of the metastable steady states, whereas *in the thermodynamic limit, the bistable phases become perfectly pure*. The two modes are either in vacuum or in a high-intensity coherent state; meanwhile the atoms are in one of their hyperfine ground states. The essential features and the phase diagram can be captured by a mean-field theory.

*vukics.andras@wigner.hu

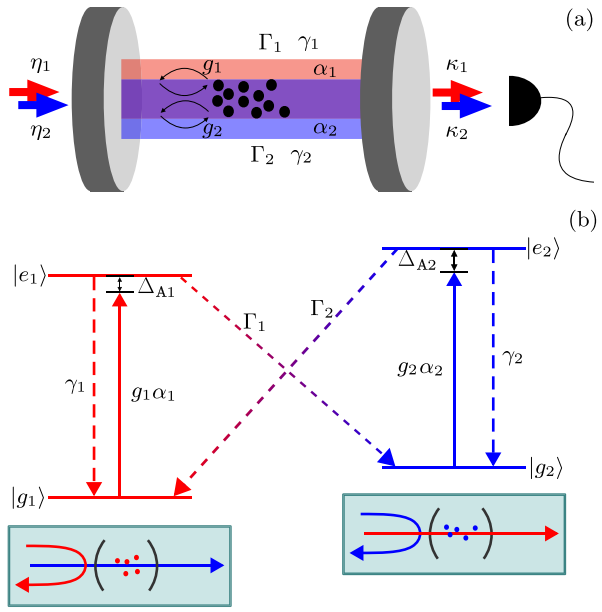

FIG. 1. (a) Parameters of the cavity QED scheme with two laser-driven modes interacting with an ensemble of atoms. The modes are spatially separated only for illustrative purposes; in practice, two fundamental modes of the cavity can be used. (b) Relevant level scheme of the atoms with two dipole-allowed transitions cross-coupled by relaxation processes. Schematic panels at the bottom represent that the atomic ground states switch the transmission or reflection of the cavity drives.

Consider a cold ensemble of N atoms interacting with two modes of a cavity with frequencies ω_{Ci} and linewidths κ_i ($i = 1, 2$ for the two modes, respectively; cf. Fig. 1). The modes are externally driven by coherent laser lights at frequencies ω_i, with drive amplitudes $\sqrt{N}\,\eta_i$, respectively. The scaling factor $\sqrt{N}$ is introduced for later convenience. The cavity modes couple to the electric dipole transitions $|g_1\rangle \leftrightarrow |e_1\rangle$ and $|g_2\rangle \leftrightarrow |e_2\rangle$, respectively. These transitions have resonance frequencies ω_{Ai} and linewidths γ_i, and the electric dipole interaction strength is expressed in terms of the single-photon Rabi frequency, $g_i = \sqrt{\frac{N\omega_{Ci}}{2\epsilon_0\hbar\mathcal{V}}}d_i$, with d_i being the atomic dipole moment, and the mode volume is $\mathcal{V}$. Note that by introducing N into the definition of the g_i, these parameters describe the collective coupling between the modes and the cold atomic ensemble.

Importantly for the scheme, atoms from the excited levels may decay not only to the cavity-coupled ground state, i.e., $|e_i\rangle \leftrightarrow |g_i\rangle$, but cross decays $|e_1\rangle \to |g_2\rangle$, $|e_2\rangle \to |g_1\rangle$ are also possible with rates Γ_1 and Γ_2, respectively. This mechanism couples the subspaces 1 and 2. The drive 1(2) is very far detuned from the transition $e_{2(1)} \to g_{2(1)}$, thus no cross-coherence is created between the states 1 and 2.

The time evolution of the dynamical variables can be described by a mean-field model using Maxwell-Bloch equations [30]. The atoms collectively couple to the cavity modes, which mediate an infinite-range interaction. As a result the mean-field theory provides an accurate description of our system. While in the case of short-range interactions the fluctuations can wash out the mean-field bistability [31], in the case of collective coupling the mean-field equations become exact in the thermodynamic limit [32].

Let $\alpha_i = \mathrm{Tr}(a_i)/\sqrt{N}$ denote the complex amplitude of the cavity field modes, where a_i is the annihilation operator of the respective cavity mode. The atomic polarization of the corresponding transition is the quantum average $m_i = \langle |g_i\rangle\langle e_i| \rangle$. In the spirit of the mean-field approximation, the atoms are not distinguished according to their coordinates or velocities in the cavity mode, so we do not need to add ensemble averaging to the collective variables. The filling ratios of the states $|g_i\rangle$ are denoted by $n_{gi} = \langle |g_i\rangle\langle g_i| \rangle$—they are numbers between 0 and 1—and n_{ei} for the states $|e_i\rangle$ are defined analogously. The mean-field equations of motion read

$$
\begin{aligned}
\dot{\alpha}_1 &= (i\Delta_{C1} - \kappa_1)\alpha_1 + g_1 m_1 + \eta_1, \\
\dot{m}_1 &= (i\Delta_{A1} - \gamma_1 - \Gamma_1)\, m_1 + g_1[n_{e1} - n_{g1}]\alpha_1, \\
\dot{n}_{e1} &= -g_1[\alpha_1^* m_1 + m_1^* \alpha_1] - 2(\gamma_1 + \Gamma_1) n_{e1}, \\
\dot{n}_{g1} &= g_1[\alpha_1^* m_1 + m_1^* \alpha_1] + 2\gamma_1\, n_{e1} + 2\Gamma_2\, n_{e2}, \qquad \text{(1a)} \\
\dot{\alpha}_2 &= (i\Delta_{C2} - \kappa_2)\alpha_2 + g_2 m_2 + \eta_2, \\
\dot{m}_2 &= (i\Delta_{A2} - \gamma_2 - \Gamma_2)\, m_2 + g_2[n_{e2} - n_{g2}]\alpha_2, \\
\dot{n}_{e2} &= -g_2[\alpha_2^* m_2 + m_2^* \alpha_2] - 2(\gamma_2 + \Gamma_2) n_{e2}, \\
\dot{n}_{g2} &= g_2[\alpha_2^* m_2 + m_2^* \alpha_2] + 2\gamma_2\, n_{e2} + 2\Gamma_1\, n_{e1}. \qquad \text{(1b)}
\end{aligned}
$$

The equations of the field mode α_i and the polarization m_i are written in a frame rotating at ω_i ($i = 1, 2$). Without loss of generality, for simplicity, we will consider a symmetric case that the parameters with index $i = 1$ and 2 are equal pairwise, $\gamma_i = \gamma$, $\Gamma_i = \Gamma$, $\kappa_i = \kappa$, and $g_i = g$ for $i = 1, 2$. We consider resonant driving of the cavity modes, $\Delta_{C1} = \Delta_{C2} = 0$. The cavity linewidth $\kappa = 1.32\gamma$ and the atom-cavity coupling are taken from the experiment [28]; for this latter the single atom coupling $g(N = 1) = 0.1\gamma$. Without loss of generality we chose $\Gamma = \gamma$. The effect of the coherent drive η_1 on the atomic variables involving state 2 scales with $(\omega_1 - \omega_2)^{-1}$, which is the inverse of the hyperfine splitting, $1/(10^3\gamma)$, and is thus negligibly small compared to the other variables. The drive amplitudes η_1 and η_2 are left to be the control parameters of the system, which can be tuned to explore different phases and transitions between them.

What we achieved with the scaling with N of the dynamical variables and parameters introduced above is that N does not appear in the system (1), not even as the upper limit of the range of the population variables. Moreover, g with the above definition (incorporating a factor of $\sqrt{N}$) makes g^2 proportional to the ensemble cooperativity $\mathcal{C} \equiv g^2/\sqrt{(\Delta_C^2+\kappa^2)(\Delta_A^2+\gamma^2)}$. This latter quantity is a measure of nonlinearity as attested by that optical bistability in a system of *two-level atoms* coupled to a cavity mode becomes possible in the $\mathcal{C} \sim 1$ regime. Note that for $\Gamma_i = 0$ the system (1) separates to two uncoupled two-level systems, where bistability would originate from the saturation of the atoms. Although we will consider large atomic detuning Δ_A with respect to the linewidth γ (for numerical calculations $\Delta_A = -12\gamma$ was chosen, where the negative sign stands for red detuning), significant excited state population n_{ei} can occur for large intensities. This possibility is taken into account in these equations. Nevertheless, in the following we will study another solution of the mean-field

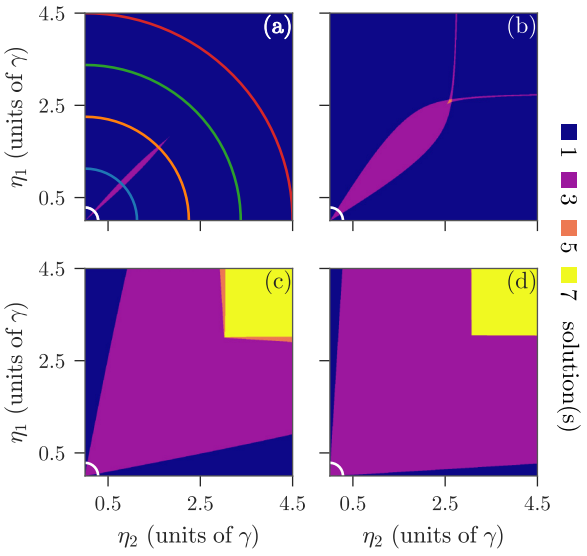

FIG. 2. Phase diagram with domains with a different number of stable solutions of the system (1) on the plane of the drive amplitudes η_1, η_2. The cooperativity increases from (a) to (d), corresponding to atom numbers $N = 5 \times 10^3$, 10^4, 10^5, and 10^6, respectively, with the single atom coupling $g(N = 1) = 0.1\gamma$. Relevant quantities along the coloured quarter circular arcs plotted on the phase diagrams are shown in Figs. 3 and 4. Radii of the colored circular arcs are $\eta/\gamma = 0.29$, 1.13, 2.25, 3.38, 4.5. The white arcs in the low drive limit are of particular interest with respect to DQPT. The symmetry to the diagonal is a consequence of the artificial choice of equal parameters for the 1 and 2 transitions.

equations which is bound to the cross-coupling decay terms and takes place in the low-excitation limit of the atoms.

The steady-state solution of Eqs. (1) can be obtained by setting the temporal derivatives on the left-hand side to zero. The remaining system of algebraic equations can be transformed into a single, seventh-order polynomial equation with real coefficients for the variable $n_{e1} - n_{g1}$. Such an equation can have 1, 3, 5, or 7 real solutions out of which, respectively, 1, 2, 3, or 4 are stable, the rest are unstable. The number of stable solutions depends on the control parameters η_1 and η_2, and domains with different numbers are depicted as a phase diagram in Fig. 2.

The phase diagram depends on the cooperativity that in the present setup can be changed by the atom number N. Whereas $N = 5 \times 10^3$ [Fig. 2(a)] allows for one or three solutions only, the large atom numbers $N = 10^5$ and 10^6 [Figs. 2(c) and 2(d)] give rise to domains with five (orange edge of the bright yellow domain) or even seven solutions (bright yellow domain). An intermediate phase diagram is obtained for $N = 10^4$ [Fig. 2(b)] where a domain with five solutions exists, but one with seven solutions does not. A closer look at the concrete solutions in the domains with five and seven solutions (not shown here) reveals that the excited states n_{ei} are significantly populated, while the polarizations m_i have low values. This means that the steady states correspond to statistical mixtures, i.e., the quantum purity of the state is low. In the following we will focus on the bottom left corner of the phase diagrams where only one or two stable solutions exist.

The different solutions in a given domain of the phase diagram are distinct in a macroscopic observable, which is the transmitted power $\kappa|\alpha_i|^2$ in our case ($i = 1, 2$). This is a suitable order parameter of phases and is readily obtained from the mean-field model. The solution (valid for our case of $\Delta_C = 0$ and $|\Delta_A| \gg \gamma + \Gamma$) reads

$$|\alpha_i|^2 = \frac{\eta_i^2}{\kappa^2} \frac{1}{1 + \mathcal{C}^2(n_{ei} - n_{gi})^2}, \tag{2}$$

highlighting the role of the cooperativity as a measure of nonlinearity [33]. The factor η_i^2/κ^2 is simply the number of photons in the resonantly driven empty cavity and will be used as a normalization factor. The second factor above can be identified as transmittance. Equation (2) is not an explicit solution as the population difference $n_{ei} - n_{gi}$ depends on the intracavity intensity $|\alpha_i|^2$. However, this form allows for getting insight into the phases.

If the population $n_{g1} \simeq 1$ and $n_{e1} \ll n_{g1}$, the transmittance through the mode 1 is suppressed for large cooperativity $\mathcal{C} \gg 1$. As there is no field in the cavity mode 1, all the atoms being in state $|g_1\rangle$ is a stable solution. On the other hand, according to the solution above with $n_{e2} \approx 0$ and $n_{g2} \approx 0$, mode 2 is closely resonantly excited, which leads to transmittance 1. Reversely, there is also a stable solution in which all the atoms are in $|g_2\rangle$, $n_{g2} \simeq 1$, and the transmittance of mode 1 is close to unity. The domain with three solutions in Fig. 2 corresponds to the case when these stable steady

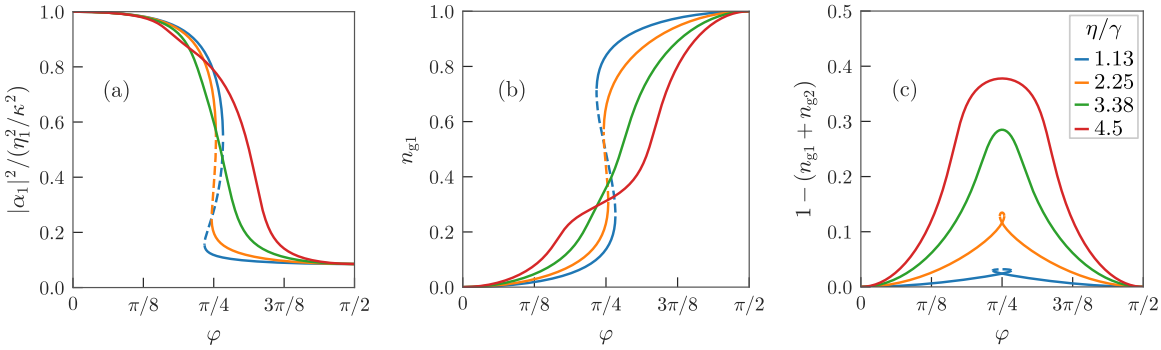

FIG. 3. Crossing domains with multiple stable solutions along the circular arcs in Fig. 2(a) ($N = 5 \times 10^3$). The transmittance of cavity for mode 1 (a) and relative atomic population (b), (c) are shown in corresponding color as a function of the arc angle φ measured from the vertical axis. Solid (dashed) lines correspond to stable (unstable) solutions.

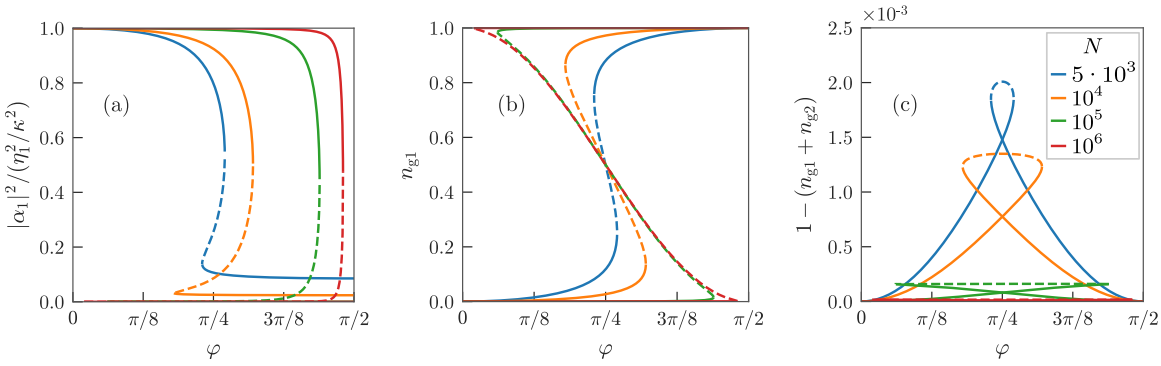

FIG. 4. Finite-size scaling to the thermodynamic limit. The order parameter represented by the transmittance of cavity for mode 1 is plotted in (a), and the relative atomic population is shown in (b) and (c) along the circular arcs on the phase space in Fig. 2(a) with a radius of $\eta/\gamma = 0.29$ for different atom numbers N. φ is measured from the vertical axis. Solid (dashed) lines correspond to stable (unstable) solutions.

states coexist. This will be further investigated along circular sections of the phase diagram, where $\eta_1^2 + \eta_2^2 \equiv \eta^2$ is constant. As the total input power per atom is proportional to $\eta_1^2 + \eta_2^2$, this section represents a fixed total drive intensity per atom, and increasing the angle $\varphi = \arctan \eta_2/\eta_1$ from 0 to $\pi/2$ corresponds to a continuous switching from driving mode 1 to 2.

Figure 3 shows cavity transmittance [Fig. 3(a)], ground state [Fig. 3(b)], and total excited state populations [Fig. 3(c)] as a function of the angle measured from axis η_1 for case $N = 5000$ along circular arcs of various radii plotted in Fig. 2(a) with the same colors. Because of the $1 \leftrightarrow 2$ symmetry of the scheme, the plot of the same quantities with index 2 gives just the mirror images of the ones with index 1; therefore only the latter is shown. The red and the green arcs do not cross the bistable region, hence there is only one real solution along those, which is, of course, stable. The rest of the curves, for both the transmittance and the ground-state population, show a characteristic S-shaped form of a bistability with overlapping stable solutions (solid line) connected by an unstable one (dashed line). The stability has been checked by means of linear perturbation analysis on Eqs. (1). High (low) transmittance corresponds to low (high) relative ground-state population. For decreasing the total input power, the S-shaped curves show convergence in Figs. 3(a) and 3(b), whereas a gradual decrease of the population in the excited states is shown in Fig. 3(c). In this limit the bistability is formed between the two hyperfine ground states, the excited states being virtually populated only underway on the two-photon transition between the ground states. One can identify thus a dissipative quantum phase transition in the spirit of the three conditions given in the introduction, where in particular, the phases correspond to quantum states of high purity.

The thermodynamic limit, where the duality of metastable phases becomes a phase transition, can be defined as $\mathcal{C} \to \infty$ while η is kept constant. In a practical case, the cooperativity can be increased by the atom number, hence the $N \to \infty$ implies that the actual drive power $N\eta^2$ has to go to infinity. The axes of the phase diagrams in Fig. 2 already used this scaling. Therefore the circular arcs of a radius $\eta/\gamma = 0.29$, plotted in each phase diagram (white), are fixed in the finite-size scaling. While the boundaries of the multivalued domain vary slightly, the phase diagram is qualitatively the same. For increasing cooperativity (via atom number), Figs. 4(a) and 4(b) show that the S-shaped curve tends to a sharper Z-shaped one (mirrored). Interestingly, when going towards the thermodynamic limit, both solutions become stable in almost the total range of the control parameter η_2/η_1. The initial condition determines which phase the system takes in the bistability domain. Even a very strong drive $\eta_{1(2)}$ cannot kick off the atoms from the state $g_{1(2)}$ because the light cannot penetrate into the cavity. Simultaneously, as shown in Fig. 4(c), the population in the excited states tends to completely vanish in this limit. Thus, in the thermodynamic limit, the proposed system has two stable solutions with the atoms being in one of the ground states $|g_{1(2)}\rangle$ and the other mode 2 (1) being populated by a coherent state, meaning that in this limit the perfect quantum purity of the phases of the system is achieved.

To summarize, we have proposed an experimentally accessible scheme of a metastability of steady states turning into true bistability, that is, a first-order dissipative quantum phase transition in a nonextensive thermodynamic limit, where moreover the phases become pure states. The four-level atomic scheme can be realized to a good approximation within the hyperfine structure of, e.g., the D2 line of rubidium 87, as discussed in [28]. The atom number can be varied in a controlled way over many orders of magnitude in an experiment, allowing thus for a finite-size scaling to the thermodynamic limit. Besides the investigation of fundamental concepts of phase transitions in mesoscopic quantum systems, the bistability between long-lived ground states holds prospects for new atomic memory architectures.

This research was supported by the Ministry of Culture and Innovation and the National Research, Development and Innovation Office within the Quantum Information National Laboratory of Hungary (Grant No. 2022-2.1.1-NL-2022-00004).

[1] E. M. Kessler, G. Giedke, A. Imamoglu, S. F. Yelin, M. D. Lukin, and J. I. Cirac, Dissipative phase transition in a central spin system, Phys. Rev. A **86**, 012116 (2012).

[2] K. Macieszczak, M. Guţă, I. Lesanovsky, and J. P. Garrahan, Towards a theory of metastability in open quantum dynamics, Phys. Rev. Lett. **116**, 240404 (2016).

[3] T. E. Lee, H. Haeffner, and M. C. Cross, Collective quantum jumps of Rydberg atoms, Phys. Rev. Lett. **108**, 023602 (2012).

[4] C. Ates, B. Olmos, J. P. Garrahan, and I. Lesanovsky, Dynamical phases and intermittency of the dissipative quantum Ising model, Phys. Rev. A **85**, 043620 (2012).

[5] M. Marcuzzi, E. Levi, S. Diehl, J. P. Garrahan, and I. Lesanovsky, Universal nonequilibrium properties of dissipative Rydberg gases, Phys. Rev. Lett. **113**, 210401 (2014).

[6] C. Carr, R. Ritter, C. G. Wade, C. S. Adams, and K. J. Weatherill, Nonequilibrium phase transition in a dilute Rydberg ensemble, Phys. Rev. Lett. **111**, 113901 (2013).

[7] N. Malossi, M. M. Valado, S. Scotto, P. Huillery, P. Pillet, D. Ciampini, E. Arimondo, and O. Morsch, Full counting statistics and phase diagram of a dissipative Rydberg gas, Phys. Rev. Lett. **113**, 023006 (2014).

[8] A. Urvoy, F. Ripka, I. Lesanovsky, D. Booth, J. P. Shaffer, T. Pfau, and R. Löw, Strongly correlated growth of Rydberg aggregates in a vapor cell, Phys. Rev. Lett. **114**, 203002 (2015).

[9] F. Letscher, O. Thomas, T. Niederprüm, M. Fleischhauer, and H. Ott, Bistability versus metastability in driven dissipative Rydberg gases, Phys. Rev. X **7**, 021020 (2017).

[10] R. Labouvie, B. Santra, S. Heun, and H. Ott, Bistability in a driven-dissipative superfluid, Phys. Rev. Lett. **116**, 235302 (2016).

[11] J. Benary, C. Baals, E. Bernhart, J. Jiang, M. Röhrle, and H. Ott, Experimental observation of a dissipative phase transition in a multi-mode many-body quantum system, New J. Phys. **24**, 103034 (2022).

[12] F. Ferri, R. Rosa-Medina, F. Finger, N. Dogra, M. Soriente, O. Zilberberg, T. Donner, and T. Esslinger, Emerging dissipative phases in a superradiant quantum gas with tunable decay, Phys. Rev. X **11**, 041046 (2021).

[13] S. R. K. Rodriguez, W. Casteels, F. Storme, N. Carlon Zambon, I. Sagnes, L. Le Gratiet, E. Galopin, A. Lemaître, A. Amo, C. Ciuti, and J. Bloch, Probing a dissipative phase transition via dynamical optical hysteresis, Phys. Rev. Lett. **118**, 247402 (2017).

[14] T. Fink, A. Schade, S. Höfling, C. Schneider, and A. Imamoglu, Signatures of a dissipative phase transition in photon correlation measurements, Nat. Phys. **14**, 365 (2018).

[15] G. Dagvadorj, M. Kulczykowski, M. H. Szymańska, and M. Matuszewski, First-order dissipative phase transition in an exciton-polariton condensate, Phys. Rev. B **104**, 165301 (2021).

[16] J. M. Fink, A. Dombi, A. Vukics, A. Wallraff, and P. Domokos, Observation of the photon-blockade breakdown phase transition, Phys. Rev. X **7**, 011012 (2017).

[17] M. Fitzpatrick, N. M. Sundaresan, A. C. Y. Li, J. Koch, and A. A. Houck, Observation of a dissipative phase transition in a one-dimensional circuit QED lattice, Phys. Rev. X **7**, 011016 (2017).

[18] R. Sett, F. Hassani, D. Phan, S. Barzanjeh, A. Vukics, and J. M. Fink, Emergent macroscopic bistability induced by a single superconducting qubit, arXiv:2210.14182.

[19] R. Bonifacio and L. A. Lugiato, Photon statistics and spectrum of transmitted light in optical bistability, Phys. Rev. Lett. **40**, 1023 (1978).

[20] R. Bonifacio and L. A. Lugiato, Bistable absorption in a ring cavity, Lett. Nuovo Cimento (1971–1985) **21**, 505 (1978).

[21] A. Dombi, A. Vukics, and P. Domokos, Optical bistability in strong-coupling cavity QED with a few atoms, J. Phys. B: At. Mol. Opt. Phys. **46**, 224010 (2013).

[22] W. Casteels, R. Fazio, and C. Ciuti, Critical dynamical properties of a first-order dissipative phase transition, Phys. Rev. A **95**, 012128 (2017).

[23] T. L. Heugel, M. Biondi, O. Zilberberg, and R. Chitra, Quantum transducer using a parametric driven-dissipative phase transition, Phys. Rev. Lett. **123**, 173601 (2019).

[24] A. Dombi, A. Vukics, and P. Domokos, Bistability effect in the extreme strong coupling regime of the Jaynes-Cummings model, Eur. Phys. J. D **69**, 60 (2015).

[25] H. J. Carmichael, Breakdown of photon blockade: A dissipative quantum phase transition in zero dimensions, Phys. Rev. X **5**, 031028 (2015).

[26] A. Vukics, A. Dombi, J. M. Fink, and P. Domokos, Finite-size scaling of the photon-blockade breakdown dissipative quantum phase transition, Quantum **3**, 150 (2019).

[27] T. W. Clark, A. Dombi, F. I. B. Williams, Á. Kurkó, J. Fortágh, D. Nagy, A. Vukics, and P. Domokos, Time-resolved observation of a dynamical phase transition with atoms in a cavity, Phys. Rev. A **105**, 063712 (2022).

[28] B. Gábor, D. Nagy, A. Dombi, T. W. Clark, F. I. B. Williams, K. V. Adwaith, A. Vukics, and P. Domokos, Ground-state bistability of cold atoms in a cavity, Phys. Rev. A **107**, 023713 (2023).

[29] E. Suarez, F. Carollo, I. Lesanovsky, B. Olmos, P. W. Courteille, and S. Slama, Collective atom-cavity coupling and nonlinear dynamics with atoms with multilevel ground states, Phys. Rev. A **107**, 023714 (2023).

[30] W. H. Louisell, *Quantum Statistical Properties of Radiation* (Wiley, New York, 1990), p. 473.

[31] H. Landa, M. Schiró, and G. Misguich, Multistability of driven-dissipative quantum spins, Phys. Rev. Lett. **124**, 043601 (2020).

[32] F. Carollo and I. Lesanovsky, Exactness of mean-field equations for open Dicke models with an application to pattern retrieval dynamics, Phys. Rev. Lett. **126**, 230601 (2021).

[33] See Supplemental Material at http://link.aps.org/supplemental/10.1103/PhysRevResearch.5.L042038 for the derivation of the mean-field equations (1), a justification of neglecting the noise in the thermodynamic limit, and the main steps to obtain Eq. (2).